Macromolecules
ARTICLE

Macromolecules **2010**, *43*, 2343–2348 **2343**
DOI: 10.1021/ma902211u

The Molecular Structure of Polymer−Fullerene Composite Solar Cells and Its Influence on Device Performance

Richard M. Beal, Alexandros Stavrinadis, Jamie H. Warner, Jason M. Smith, Hazel E. Assender, and Andrew A. R. Watt*

Department of Materials, University of Oxford, South Parks Rd, Oxford, U.K.

Received October 6, 2009; Revised Manuscript Received February 2, 2010

ABSTRACT: Understanding the nanomorphology of polymer-based solar cells is key to improving device efficiencies. A detailed study of the changes in polymer solar cell morphology at the molecular level and in real time under process conditions is presented. Using low voltage, high resolution electron microscopy (LVHREM) we observe the mechanisms of PCBM-rich domain migration in real time and provide evidence for vertical segregation within the bulk heterojunction and increased crystallinity of both P3HT and PCBM. The results of the study highlights the fact that P3HT:PCBM bulk heterojunction morphology should be viewed within the framework of a four-phase, three-dimensional, nonequilibrium system.

1. Introduction

Understanding the nanomorphology of polymer-based solar cells has become increasingly important in recent years since the discovery that a simple post production anneal can lead to efficiency gains of over 100%.[1,2] Although the annealing step has some interfacial benefits,[2−4] it is the changes that occur within the morphology of the photoactive layer itself that have garnered the most investigative attention.[5−7] Of particular interest is the system containing the conjugated polymer poly(3-hexylthiophene) (P3HT) and the fullerene derivative [6,6]-phenyl-C_{61}-butyric acid methyl ester (PCBM), which has produced some of the most advanced plastic-based solar cells to date.[2,8] Further advancements will be greatly assisted by techniques capable of revealing the physical effects of the annealing process and relating them to the system's electronic properties. Electron microscopy techniques are well established in the inorganic semiconductor industry for this purpose, but techniques for the determination of molecular structure in organic electronics are not well developed. This is largely due to problems with sample preparation and electron knock-on damage from high-voltage electron beams. In this paper, we use low voltage, electron microscopy to achieve high resolution micrographs that reveal, in unprecedented detail, lateral and vertical morphologies before, after, and even during the annealing process.

In the devices under investigation, P3HT and PCBM are blended in a single layer (see Figure 1a) to form a bulk heterojunction. Absorption of a photon generates an electron−hole bound pair (exciton) which diffuses to a P3HT:PCBM interface and dissociates into separate charge carriers. The exciton has a diffusion length of 10−20 nm, which sets a limit on the allowable level of P3HT−PCBM phase separation. Once separated, the charge carriers require a bicontinuous pathway through which they can drift to their respective electrodes; holes through the polymer and electrons through the PCBM. Increased levels of structural and electronic order within these two phases are desirable for improved charge carrier mobility and extraction and subsequently, device efficiency.

Consequently, understanding and controlling the distribution and mixing of P3HT and PCBM on the nanometer scale are of paramount importance for the development of high efficiency plastic solar cells. Early work that focused on optimizing the P3HT:PCBM morphology used AFM to show that the choice of solvent could greatly affect the PCBM-rich domain size in spin-cast P3HT:PCBM films.[6,9] More recently, low resolution TEM and optical studies have shown that annealing leads to a coarsening of the P3HT:PCBM interphase penetration[2] and over extended periods of time, the formation of PCBM crystallites with micrometer dimensions.[3,5,9,10] The formation of such large crystallites is undesirable in solar cells as the larger domain size increases the risk of germinate recombination and leads to increased photoluminescence.[1,5,11] Nonetheless, a certain level of nanoscale coarsening is desirable to improve the bicontinuous morphology necessary for efficient charge transport.[2] In addition, vertical segregation within the P3HT:PCBM layer has been proposed by a number of authors[12,13] and most recently characterized by variable angle spectroscopic ellipsometry (VASE).[5] This is supported by secondary ion mass spectroscopy (SIMS)

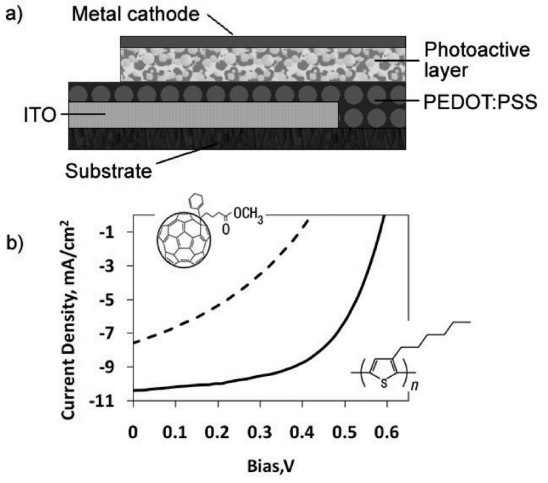

Figure 1. Current voltage curves and schematic of polymer-based solar cell. (a) Schematic of a polymer-based solar cell showing the planar layered architecture. (b) Current voltage curve of a typical P3HT:PCBM solar cell preanneal (dotted line) and postanneal (full line). Insets are of PCBM (top left) and P3HT.

*Corresponding author. E-mail: andrew.watt@materials.ox.ac.uk.

Published on Web 02/12/2010

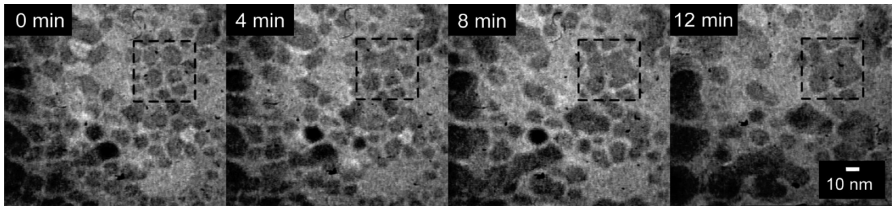

Figure 2. Low voltage, high resolution transmission electron micrograph time series of a P3HT:PCBM blend during the annealing process. The highlighted area shows one area of PCBM domain agglomeration.

experiments conducted on polyfluorene:PCBM films on silicon, which revealed a four-layer morphology with the upper layers enriched with polymer and the substrate interface enriched with PCBM.[14]

Annealing can also improve the crystallinity of both P3HT and PCBM. This has been inferred from a number of experimental techniques including UV−vis absorption,[3] external quantum efficiency (EQE) spectra,[5] X-ray diffraction,[2,7,15,16] transmission electron microscopy,[1] electron diffraction,[15,17,18] Raman spectroscopy[19] and spectroscopic ellipsometry.[11] Films of neat P3HT exhibit a natural tendency to self-organize into crystalline lamellae but this is inhibited by the addition of PCBM.[15] However, heating of P3HT:PCBM films to temperatures above the P3HT glass transition temperature facilitates phase separation which then allows the enlarged P3HT domains to crystallize. Diffraction studies[7,15] suggest there is a preferential orientation of the P3HT lamellae with the polymer backbone parallel to the substrate and the hexyl side chains normal to the substrate. Although the cause of this preferred alignment is not fully understood, it has been hypothesized that at least in the vicinity of the substrate−polymer interface, interactions between the hydrophobic P3HT side-chains and the hydrophilic SiO_2 substrate may be causative.[11] Similar orientation has been observed in P3HT:PCBM layers spun cast on top of PEDOT:PSS.[16]

The body of evidence regarding annealing induced crystallization of PCBM is more equivocal. Pristine PCBM is even more likely to crystallize than P3HT and has been shown to readily form thin films of densely and homogeneously distributed nanocrystals when spin-cast.[20] However, XRD analysis of P3HT:PCBM blend films has noted a distinct lack of PCBM crystallinity even after annealing,[16] which suggests that the polymer chains play an inhibitory role. The failure to observe PCBM crystallites by XRD is puzzling considering that PCBM crystals have been identified in P3HT:PCBM films by TEM[1,18] and electron diffraction,[17,18] which matches well with PCBM crystallite formation reported in other conjugated polymer systems.[21]

Further advancements in organic solar cell efficiencies will be greatly assisted by techniques designed to understand and relate their physical and electronic properties. Electron microscopy techniques are well established in the inorganic semiconductor industry for this purpose, but techniques for the determination of molecular structure in organic electronics are not well developed. This is largely due to problems with sample preparation and electron knock-on damage from high-voltage electron beams. In this paper, we use low voltage electron microscopy and apply a simple sample preparation technique to characterize the nanostructure of a donor−acceptor polymer composite and relate this to device performance.

2. Results and Discussion

Figure 1a shows the device geometry used in this study while Figure 1b shows the current−voltage characteristics of a P3HT:PCBM solar cell before and after the thermal anneal step. The dramatic increase in short circuit current, fill factor, and open circuit voltage are all apparent and result in an efficiency increase from 1.3% to 4.0%. The anneal step induces an enhanced molecular mobility which allows rearrangement of both P3HT polymer chains and PCBM molecules. This leads to the coarsening of morphology as has been shown previously by low resolution TEM.[2] To further investigate the dynamics of this process we annealed a P3HT:PCBM solar cell sample at 150 °C while simultaneously imaging by TEM (details can be found in the Experimental Section). The time series of images in Figure 2 gives insight into how the morphological rearrangement of P3HT and PCBM occurs. At the beginning of the anneal process the morphology is dominated by sub 10 nm diameter PCBM-rich domains immersed in a P3HT-rich matrix. The contrast in gray scale can be attributed to the relative densities of P3HT and PCBM[17] with the denser PCBM (1.5 g cm^{-3})[22] appearing darker than the P3HT (1.10 g cm^{-3}).[23] Of immediate interest is that at this scale, the PCBM-rich phase is noncontinuous with an average nearest neighbor distance (width of the P3HT matrix between adjacent PCBM domains) of 1.3 ± 0.6 nm. Virtually all of the excitons generated within the polymer are within diffusion range of a P3HT:PCBM heterojunction where electron transfer occurs on the picosecond time scale.[24] Once separated, however, it appears that electron transport must be reliant on nonconductive mechanisms such as hopping and tunneling to migrate from one domain to the next.

The images show that upon annealing, the PCBM-rich domains present in the pristine film begin to agglomerate. This in turn allows larger volumes of P3HT-rich matrix to form. After 12 min the average area of individual PCBM-rich domains increases from 143 ± 44 to 350 ± 110 nm^2. Despite this, the PCBM domain nearest neighbor distance remains at 1.8 ± 0.8 nm—a statistically insignificant change. The upshot is that the rate limiting charge transport step between PCBM domains is not particularly affected by the coarsening, as the average nearest neighbor distance remains fairly constant. Yet the agglomeration of adjacent domains does mean that separated electrons are required to transit between domains less frequently. The net result is an improvement in fullerene mobility within the device.

An analysis of the area fractions of the dark and light phases shows that the total area fractions remain constant over time. This suggests that the coarsening of the PCBM-rich domain size is not due to phase separation of PCBM from the P3HT-rich matrix, but instead can be accounted for solely by the agglomeration of PCBM-rich domains present in the as cast film.

Recent *in situ* ellipsometry experiments have suggested that the annealing of P3HT:PCBM blends induces immediate crystallization of P3HT followed by subsequent diffusion of PCBM.[5] The authors hypothesized that crystallization of P3HT facilitated diffusion of PCBM through low-polymer-density pathways that are created between P3HT crystallites. The work presented here suggests an alternative mechanism for PCBM mobility, with entire PCBM-rich nanodomains migrating and agglomerating in order to decrease the interfacial area of the morphology.

The resolution of the micrographs in Figure 2 was limited due to the thermal motion induced by the annealing process. In order to further explore the P3HT:PCBM morphology, additional, higher resolution TEM images were taken of samples from

pristine and postanneal devices and representative images are presented in Figure 3

This result is slightly different to that observed in Figure 2 and we suggest that this is due to the difference in anneal conditions, Figure 2 is in situ, under vacuum and suspended across a hole in a carbon film whereas Figure 3 is ex situ, at room pressure and suspended on a glass:ITO substrate.

Figure 3a shows the pristine morphology of sub 10 nm PCBM-rich domains in a P3HT matrix, familiar from images in Figure 2. The PCBM domain nearest neighbor distance was calculated as 1.7 ± 0.5 nm. In sharp contrast to this is the morphology observed in the annealed sample (Figure 3b). The PCBM-rich regions have agglomerated into larger, denser, more irregular shapes and the average nearest neighbor distance was measured as 2.8 ± 1.1 nm. There are larger unbroken volumes of P3HT-rich phase, with excitons now having to diffuse up to 20 nm to reach a heterojunction. Without the thermal motion from the heating stage blurring the images, finer features of the morphology are brought into focus, such as evidence for the formation of lamellae structures within the P3HT phase, which are indicative of P3HT crystallization. The micrographs in Figure 3 bear a remarkable resemblance to schematic representations of annealing induced changes envisioned by Erb et al.[16] and the average lamellae domain size of 8 ± 0.5 nm in Figure 3b fits nicely with the size previously calculated for P3HT lamellae from XRD measurements using Scherrer's relation.[16] This result is slightly different to that observed in Figure 2, and we suggest that this is due to the difference in anneal conditions, Figure 2 is in situ, under vacuum and suspended across a hole in a carbon film whereas Figure 3 is ex situ, at room pressure and suspended on a glass:ITO substrate.

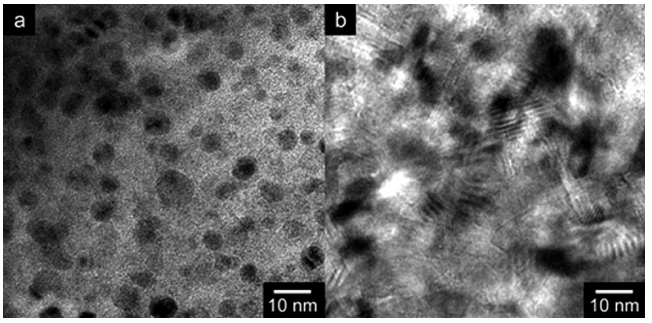

Figure 3. Low voltage, high resolution transmission electron micrographs of P3HT:PCBM blends. (a) Bright micrograph of P3HT:PCBM solar cell before annealing. (b) Bright field micrograph of P3HT:PCBM solar cell after annealing at 150 °C for 10 min.

It is worth noting the relatively sparse distribution of P3HT lamella, which explains the modest P3HT crystal peaks observed in XRD spectra of P3HT:PCBM devices.[2] An area analysis using Vistametrix yields only $12 \pm 1\%$ P3HT crystallinity by area. This highlights that even for P3HT, a relatively crystalline polymer, the amorphous phase is largely dominant. It is clear that that considerable opportunity exists for the development of conjugated polymers that are either capable of superior crystallinity when mixed with PCBM or that are not reliant on high levels of crystallinity in order to achieve high hole mobilities

Higher resolution TEM images were analyzed to probe the various P3HT lamellae structures observed. In Figure 4, gray scale images of a lamellae region (Figure 4b) reveal a periodicity of 1.7 nm which matches reasonably well with the 1.64 nm *a*-axis spacing of the (001) reflection, as observed in XRD studies of P3HT.[2,16] As the hexyl side chain is only 0.75 nm long, the *d*-spacing suggests there is no interdigitation of the side chains. In Figure 4d, we see further evidence of P3HT crystallization with an HRTEM image showing P3HT *b*-axis stacking which corresponds to the (002) reflection.[10] The *d*-spacing of 0.38 nm, as shown in 4e and 4f, matches well with values reported elsewhere in the literature.[2,16]

PCBM crystallization was also investigated and the results are presented in Figure 5. Pre-anneal (Figure 5a), the morphology shows no obvious sign of long-range crystalline ordering. A two-dimensional fast Fourier transform (2DFFT) image of the pristine sample presents a diffuse ring with a diameter of 0.38 nm. We speculate that this is due to the P3HT conformation and corresponds to the hexyl side-chain separation, however the spacing is almost identical to the surrounding holey amorphous carbon which supports the specimen. As previously mentioned, spin-cast PCBM readily forms homogeneous films of

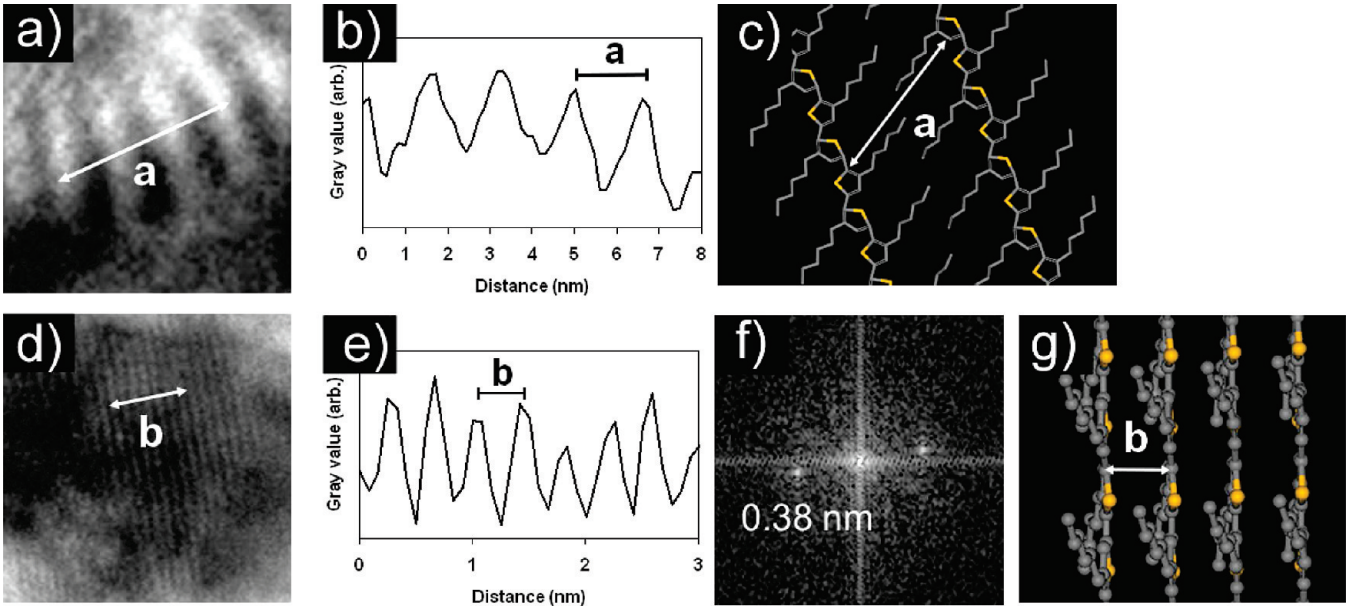

Figure 4. Low voltage, high resolution, bright field transition electron micrographs, gray scale plots, 2DFFT patterns and computer models of P3HT and PCBM crystal structures. (a, d) Bright field micrograph of a P3HT lamellae. (b) Gray scale plot of line a in part a showing lamella spacing of 1.7 nm. (c) Schematic of P3HT lamella showing *a*-axis spacing. (e) Gray scale plot of line b in part d showing lamella spacing of 0.38 nm, consistent with (020) spacing. (f) 2DFFT of part d showing *d*-spacing of 0.38 nm. (g) Computer simulation of P3HT *b*-axis spacing.

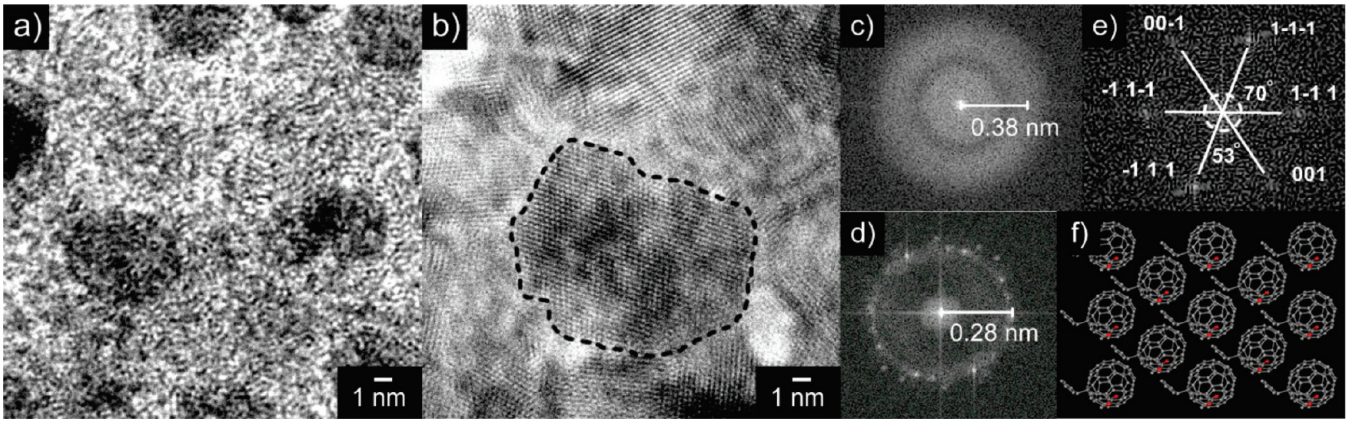

Figure 5. Low voltage, high resolution transmission electron micrographs and 2DFFT patterns of P3HT:PCBM blends showing evidence of PCBM crystallinity. (a) Bright field micrograph of P3HT:PCBM solar cell active layer before annealing. (b) Bright field micrograph of P3HT:PCBM solar cell active layer after annealing showing a characteristic PCBM crystallite within the dotted line. (c) Two dimensional fast Fourier transforms (2DFFT) of (a). (d) 2DFFT pattern of (b) revealing a *d*-spacing of 0.28 nm. The defocus value was kept constant for both images (a and b) to ensure a direct comparison. A through focal series was also taken to ensure that no lattice fringes were present in Figure 3a. (e) 2DFFT of a single PCBM crystal in (b) showing reflections that correspond to the (001) and (111) planes of PCBM's FCC structure. (f) 2D planar model of PCBM crystal packing viewed down the [110] zone axis.

nanocrystals,[9] which suggests that the PCBM domains in the as-cast P3HT:PCBM film are not pure PCBM, but contain a fraction of P3HT which inhibits crystallization.

The post anneal image (Figure 5b) shows the formation of PCBM crystallites, bordered by an amorphous matrix. The shape of the grain near the center of the image (dotted line) suggests that it has been formed by the agglomeration of two PCBM-rich domains. Furthermore, the crystalline structure is continuous, with no sign of a grain boundary which suggests that the PCBM domains agglomerated first and then crystallized as a single unit. The 2DFFT of Figure 5b is shown in Figure 5d and reveals a *d*-spacing of 0.28 nm which matches well with previously published *d*-spacings for PCBM.[20,25] The absence of the 0.28 nm feature in the 2DFFT image of the pristine sample (Figure 5c) suggests a complete lack of PCBM crystallinity in the pre annealed device and suggests that the annealing step is vital for the formation of pure PCBM crystals in these devices.

Figure 5e shows the 2DFFT obtained from the HRTEM image in Figure 5b. The two sets of spots present match the (001) and (111) planes for PCBM with an FCC crystal structure. The HRTEM images and 2DFFT analysis of the PCBM domains were compared to C_{60} crystals with known FCC crystal structure (see Supporting Information), and it was found that the structures were similar. Figure 5f shows a schematic model of the PCBM FCC structure viewed down the [110] zone axis. These results agree well with previous studies on PCBM crystal structure.[26]

The annealing induced morphological changes in polymer composite solar cells are three-dimensional. However, to date, investigations of morphological changes within the vertical plane are relatively scarce. It has been shown in both polymer−polymer blend devices[27] and vacuum deposited molecular solar cell[28] that vertical segregation can have beneficial effects on device efficiency with increased concentrations of the electron donor toward the anode, and increased concentrations of the electron acceptor toward the cathode. It is expected that a similar vertical segregation profile would benefit P3HT:PCBM devices. Models based on VASE have recently been developed which suggest that as cast films of P3HT:PCBM present an undesirable, or negative, vertical concentration profile with increased P3HT near the aluminum cathode and increased PCBM nearer the PEDOT:PSS anode.[5] Annealing moderately improves this profile although the concentration gradients are still mildly negative. With TEM we can build a picture of the vertical morphology by

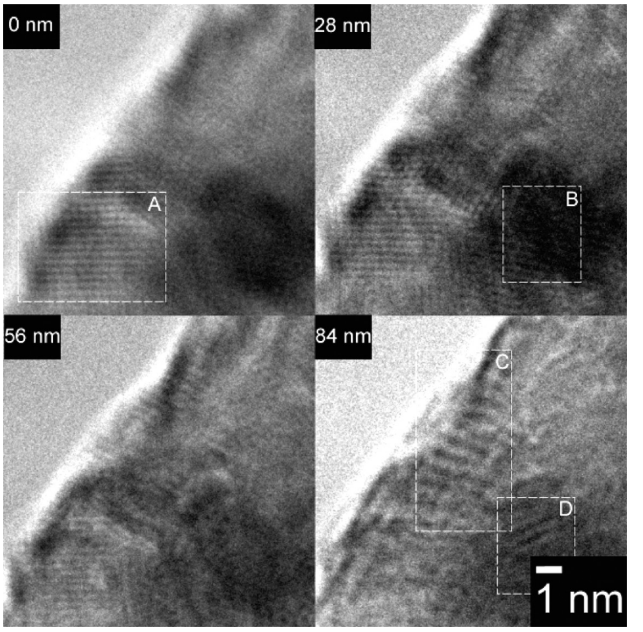

Figure 6. Low voltage, high resolution transmission electron focal series of P3HT:PCBM blend. Parts a and b are PCBM crystals. Parts c and d are P3HT lamella. The distances quoted refer to microscope focal depth.

using focal series imaging. Selecting a large, flat piece of an annealed composite film overhanging a hole in the TEM grid we executed a focal series projection vertically through the film as shown in Figure 6. In order to understand the effect of defocus on the HRTEM images of P3HT lamella and ensure that structural changes are a function of depth and not the fundamental optical response of the microscope image simulations were performed using JEMS software and are provide in Supporting Information. Evidence of vertical segregation is clear with the images taken of the surface and at a focal depth of 0 and 28 nm revealing PCBM crystals, while the image taken at a focal depth of 84 nm reveals P3HT lamellae.

Although the particles under examination are arranged randomly on the TEM grid due to the preparation technique, by focusing on a large flat particle we can be fairly certain that the focal series penetrates perpendicular to the plane of the device,

and the focal depths achieved, i.e., up to 84 nm, suggest we are viewing through the entire thickness of the active layer. However, due to the random vertical orientation, we are unable to tell whether we are looking from the top down or the bottom up. Nevertheless, if one assumes that the layer is being viewed from the bottom up (i.e., the film is upside down) the images match well with the results of previously mentioned VASE experiments[5] that suggested vertical segregation with increased PCBM concentrations near the substrate (Figure 6, parts a and b) and increased P3HT in the upper layers (c and d). More recently, investigations using electron tomography (ET) have allowed a three-dimensional rendering of a P3HT:PCBM active layer.[18] This 3D image was then "sliced" at regular intervals in order to investigate the vertical concentration profile for P3HT. These results contradict the previously mentioned VASE study by suggesting an increased P3HT concentration near the PEDOT:PSS anode. It is worth noting that both the current study and the VASE experiments used devices spin-cast from chlorobenzene, while the ET study used devices spin-cast from dichlorobenzene. As previously mentioned, research regarding vertical segregation within these devices is relatively scarce and further investigations are warranted.

3. Conclusion

In this study, we have used low voltage, high resolution TEM to reveal the mechanism of PCBM domain migration which underpins this morphological rearrangement. In addition, we have presented images of unprecedented detail that give direct confirmation of P3HT and PCBM crystallization and vertical segregation within P3HT:PCBM solar cells. The work presented shows that low voltage, high resolution electron microscopy can provide valuable insight in to the molecular level organization of materials traditionally thought of as difficult from an electron microscopy point of view. While this study has focused on the P3HT:PCBM photovoltaic system, the general technique is applicable to a broad range of soft material systems.

4. Experimental Section

Device Fabrication. P3HT (10 mg/mL, Reike Metals Inc., 4002-E) and PCBM (8 mg/mL, Nano-C, PCBM-CF) were dissolved in Chlorobenzene (Sigma, anhydrous, 99.8%) and stirred overnight at ambient temperature. ITO coated glass substrates (PGO, CEC005, $\leq 5\ \Omega$/sq.) were etched in a solution of H_2O, HCl and HNO_3 (25:25:2 vol) at 50 °C for 8 min. The substrates were then sonicated in detergent solution and deionized water before being washed in acetone and isopropyl alcohol. The substrates were then dried at ambient temperature in a nitrogen glovebox ($\leq$1 ppm of O_2, $\leq$2 ppm of H_2O) overnight. Substrates were removed from the glovebox and plasma etched with O_2 for 4s. PEDOT:PSS (Baytron P) was filtered through a 0.45 μL syringe filter (Millex Millipore, 25 mm, nylon) then spun cast at 5000 rpm for 30s. Following this, the devices were placed on a hot plate for 10 min at 140 °C in ambient atmosphere. The devices were then transported into the glovebox where a P3HT:PCBM layer was spun cast at 700 rpm for 15s. Next, the devices were transferred to a vacuum chamber where Al electrodes (70 nm) were deposited at a pressure of 2.5×10^{-7} Torr. The annealed device was then placed on a hot plate in the glovebox and annealed for 10 min at 150 °C. Each device had an area of 3 mm^2.

***I*−*V* Characterization.** Current density−voltage (*I*−*V*) curves were determined using a KH Steuernagel solar simulator (80 mW/cm^2) fitted with an AM1.5G filter) and a Keithley 2400 SMU. The light intensity at the sample position was determined with a microprocessor-based power meter (Thermo-Oriel Instruments, Model No.70260) calibrated according to ASTM standards. The solar simulator spectrum was measured with an Ocean Optics USB2000 UV−vis spectrometer.

HRTEM analysis was performed on a JEOL-JEM 4000EX LaB6 microscope with an information limit of 0.12 nm at an accelerating voltage of 100 kV and calibrated using lead sulfide nanocrystals with well-defined lattice spacings (see Supporting Information). Samples were prepared as follows: Part of the device active layer was scrapped off its substrate using a scalpel, and sonicated in dichloromethane (a bad solvent for both PCBM and P3HT) for 3 min. The resulting micrometer sized dispersion was then drop-cast onto lacey carbon film-coated copper grids. The sonication was necessary in order to create particles with edges thin enough to allow high resolution TEM at low accelerating voltages. Samples were prepared from actual devices in order to ensure the observed morphologies were truly characteristic. A sufficient number of flakes adhered to the TEM grid and overhung holes in the lacey carbon film to allow TEM analysis. For the *in situ* heat treatment, the sample was placed in a sample holder with a closed loop heating system. The sample holder was ramped to 150 °C and then imaging was initiated. To ensure that the composite morphology is not altered by electron beam damage a series of images under constant electron beam conditions where taken over a 12 min period and are detailed in Supporting Information.

Acknowledgment. The authors thanks the Rhodes Trust for their funding and support during the completion of this work.

Supporting Information Available: Text discussing the calibration of the microscope, a table of calibration data, and figures showing a high resolution transmission electron micrograph of a lead sulfide nanocrystal, effect of 100 kV electron beam on polymer film, high resolution transition electron micrographs, atomistic supercell of P3HT lamella, image simulations of lamella supercells, a side chain supercell diagram, and image simulation of side chain supercell. This material is available free of charge via the Internet at http://pubs.acs.org.

References and Notes

(1) Reyes-Reyes, M.; Kim, K.; Dewald, J.; Lopez-Sandoval, R.; Avadhanula, A.; Curran, S.; Carroll, D. L. *Org. Lett.* **2005**, *7*, 5749–5752.
(2) Ma, W. L.; Yang, C. Y.; Gong, X.; Lee, K.; Heeger, A. J. *Adv. Funct. Mater.* **2005**, *15*, 1617–1622.
(3) Chirvase, D.; Parisi, J.; Hummelen, J. C.; Dyakonov, V. *Nanotechnology* **2004**, *15*, 1317–1323.
(4) Ahn, T.; Lee, H.; Han, S. H. *Appl. Phys. Lett.* **2002**, *80*, 392–394.
(5) Campoy-Quiles, M.; Ferenczi, T.; Agostinelli, T.; Etchegoin, P. G.; Kim, Y.; Anthopoulos, T. D.; Stavrinou, P. N.; Bradley, D. D. C.; Nelson, J. *Nat. Mater.* **2008**, *7* (2), 158–164.
(6) Shaheen, S. E.; Brabec, C. J.; Sariciftci, N. S.; Padinger, F.; Fromherz, T.; Hummelen, J. C. *Appl. Phys. Lett.* **2001**, *78*, 841–843.
(7) Kim, Y.; Cook, S.; Tuladhar, S. M.; Choulis, S. A.; Nelson, J.; Durrant, J. R.; Bradley, D. D. C.; Giles, M.; McCulloch, I.; Ha, C. S.; Ree, M. *Nat. Mater.* **2006**, *5* (3), 197–203.
(8) Kim, J. Y.; Lee, K.; Coates, N. E.; Moses, D.; Nguyen, T. Q.; Dante, M.; Heeger, A. J. *Science* **2007**, *317* (5835), 222–225.
(9) Rispens, M. T.; Meetsma, A.; Rittberger, R.; Brabec, C. J.; Sariciftci, N. S.; Hummelen, J. C. *Chem. Commun.* **2003**, *17*, 2116–2118.
(10) Swinnen, A.; Haeldermans, I.; vande Ven, M.; D'Haen, J.; Vanhoyland, G.; Aresu, S.; D'Olieslaeger, M.; Manca, J. *Adv. Funct. Mater.* **2006**, *16*, 760–765.
(11) Zhokhavets, U.; Erb, T.; Hoppe, H.; Gobsch, G.; Sariciftci, N. S. *Thin Solid Films* **2006**, *496*, 679–682.
(12) Kim, Y.; Choulis, S. A.; Nelson, J.; Bradley, D. D. C.; Cook, S.; Durrant, J. R. *Appl. Phys. Lett.* **2005**, *86*, 6.
(13) Waldauf, C.; Morana, M.; Denk, P.; Schilinsky, P.; Coakley, K.; Choulis, S. A.; Brabec, C. J. *Appl. Phys. Lett.* **2006**, *89*, 23.
(14) Bjorstrom, C. M.; Bernasik, A.; Rysz, J.; Budkowski, A.; Nilsson, S.; Svensson, M.; Andersson, M. R.; Magnusson, K. O.; Moons, E. *J. Phys.: Condens. Matter* **2005**, *17*, L529–L534.
(15) Vanlaeke, P.; Swinnen, A.; Haeldermans, I.; Vanhoyland, G.; Aernouts, T.; Cheyns, D.; Deibel, C.; D'Haen, J.; Heremans, P.; Poortmans, J.; Manca, J. V. *Sol. Energy Mater. Sol. Cells* **2006**, *90*, 2150–2158.

(16) Erb, T.; Zhokhavets, U.; Gobsch, G.; Raleva, S.; Stuhn, B.; Schilinsky, P.; Waldauf, C.; Brabec, C. J. *Adv. Funct. Mater.* **2005**, *15*, 1193–1196.
(17) Yang, X. N.; Loos, J.; Veenstra, S. C.; Verhees, W. J. H.; Wienk, M. M.; Kroon, J. M.; Michels, M. A. J.; Janssen, R. A. J. *Nano Lett.* **2005**, *5*, 579–583.
(18) Bavel, S. S. v.; Sourty, E.; With, G. d.; Loos, J. *Nano Lett.* **2009**, *9*, 507–513.
(19) Klimov, E.; Li, W.; Yang, X.; Hoffmann, G. G.; Loos, J. *Macromolecules* **2006**, *39*, 4493–4496.
(20) Yang, X. N.; van Duren, J. K. J.; Rispens, M. T.; Hummelen, J. C.; Janssen, R. A. J.; Michels, M. A. J.; Loos, J. *Adv. Mater.* **2004**, *16*, 802.
(21) Yang, X. N.; van Duren, J. K. J.; Janssen, R. A. J.; Michels, M. A. J.; Loos, J. *Macromolecules* **2004**, *37*, 2151–2158.
(22) Bulle-Lieuwma, C. W. T.; van Gennip, W. J. H.; van Duren, J. K. J.; Jonkheijm, P.; Janssen, R. A. J.; Niemantsverdriet, J. W. *Appl. Surf. Sci.* **2003**, *203*, 547–550.
(23) Prosa, T. J.; Winokur, M. J.; Moulton, J.; Smith, P.; Heeger, A. J. *Macromolecules* **1992**, *25*, 4364–4372.
(24) Sariciftci, N. S.; Smilowitz, L.; Heeger, A. J.; Wudl, F. *Science* **1992**, *258* (5087), 1474–1476.
(25) Savenije, T. J.; Kroeze, J. E.; Yang, X.; Loos, J. *Thin Solid Films* **2006**, *511−512*, 2–6.
(26) Hoppe, H.; Sariciftci, N. S. *J. Mater. Chem.* **2006**, *16*, 45–61.
(27) Arias, A. C.; Corcoran, N.; Banach, M.; Friend, R. H.; MacKenzie, J. D.; Huck, W. T. S. *Appl. Phys. Lett.* **2002**, *80*, 1695–1697.
(28) Barry, P. R.; Jiangeng, X.; Soichi, U.; Stephen, R. F. *J. Appl. Phys.* **2005**, *98*, 124902.